

AperTO - Archivio Istituzionale Open Access dell'Università di Torino

In vitro drug metabolism by C-terminally truncated human flavin-containing monooxygenase 3

This is the author's manuscript

Original Citation:

Availability:

This version is available <http://hdl.handle.net/2318/89575> since

Published version:

DOI:10.1016/j.bcp.2011.11.029

Terms of use:

Open Access

Anyone can freely access the full text of works made available as "Open Access". Works made available under a Creative Commons license can be used according to the terms and conditions of said license. Use of all other works requires consent of the right holder (author or publisher) if not exempted from copyright protection by the applicable law.

(Article begins on next page)



UNIVERSITÀ DEGLI STUDI DI TORINO

This Accepted Author Manuscript (AAM) is copyrighted and published by Elsevier. It is posted here by agreement between Elsevier and the University of Turin. Changes resulting from the publishing process - such as editing, corrections, structural formatting, and other quality control mechanisms - may not be reflected in this version of the text. The definitive version of the text was subsequently published in *Biochem. Pharm.* Volume 83, 2012, DOI: [10.1016/j.bcp.2011.11.029](https://doi.org/10.1016/j.bcp.2011.11.029).

You may download, copy and otherwise use the AAM for non-commercial purposes provided that your license is limited by the following restrictions:

- (1) You may use this AAM for non-commercial purposes only under the terms of the CC-BY-NC-ND license.
- (2) The integrity of the work and identification of the author, copyright owner, and publisher must be preserved in any copy.
- (3) You must attribute this AAM in the following format: Creative Commons BY-NC-ND license (<http://creativecommons.org/licenses/by-nc-nd/4.0/deed.en>), [+ *Digital Object Identifier link to the published journal article on Elsevier's ScienceDirect® platform*]

**In vitro drug metabolism by C-terminally truncated human flavin-containing
monooxygenase 3**

Gianluca Catucci^a, Gianfranco Gilardi^a, Lars J.C. Jeuken^b and Sheila J. sadeghi^{a,*}

Department of Life Sciences and Systems Biology, University of Torino, Italy^a,

Institute of Membrane and Systems Biology, University of Leeds, United Kingdom^b.

Address correspondence to: S. Sadeghi, Department of Life Sciences and Systems Biology, Via
Accademia Albertina 13, 10123 Torino, Italy. Phone: +39-011-6704528, Fax: +39-011-
6704643.

e-mail: sheila.sadeghi@unito.it

Classification: Pharmacokinetics and Drug Metabolism

ABSTRACT

Human flavin-containing monooxygenase 3 (hFMO3) is a microsomal drug-metabolizing monooxygenase enzyme that catalyses the NADPH-dependent oxygenation of a wide range of drugs and xenobiotics which contain a soft-nucleophile, usually sulphur or nitrogen. As the release from the microsomal membranes can facilitate the *in vitro* experimental determination of drug metabolism by hFMO3, in this work we identified and eliminated the membrane anchoring sequence without affecting the activity of the enzyme and producing a soluble active enzyme. The truncated hFMO3 carrying a C-terminal deletion of 17 amino acid deletion (tr-hFMO3) was expressed and purified from the cytosolic fraction. The tr-hFMO3 proves to be detached from the membrane, properly folded and fully active towards well-known marker substrates such as benzydamine and sulindac sulfide with measured apparent K_m values of $45 \pm 8 \mu\text{M}$ and $25 \pm 4 \mu\text{M}$, respectively. Its activity was further tested with newly discovered Aurora kinase inhibitors, Tozasertib and Danusertib, and compared to those of the wild type enzyme.

The use of this soluble form of the hFMO3 enzyme as opposed to the usual microsomal preparations can be advantageous for *in vitro* drug metabolism studies that are a requirement in the early phases of drug development by pharmaceutical industry.

Keywords: flavin-containing monooxygenase, molecular docking, *in vitro* expression, drug metabolism, protein engineering, enzyme catalysis.

1. Introduction

The flavin-containing monooxygenases comprise a family of five functional enzymes and are the second most important phase 1 drug-metabolizing enzyme family after cytochromes P450 [1,2]. One member of the family, human flavin-containing monooxygenase 3 (hFMO3) is predominantly expressed in the liver where its substrates, generally nitrogen-, sulphur- and phosphorous-containing soft nucleophiles are transformed into more polar and excretable metabolites [3]. Human FMO3 contributes to the metabolism of many drugs such as ranitidine, cimetidine, tamoxifen, clozapine, benzydamine, amphetamine and mutations in its gene sequence have revealed polymorphisms that can cause significant differences in metabolism and lead to disease, one example of which is trimethylaminuria [4-6]. The enzyme is anchored to the smooth endoplasmic reticulum membrane, where its reduced flavin group binds molecular oxygen and is thought to act as a loaded gun ready to perform nucleophilic attack on the substrates [7-9].

To date the three-dimensional structure of hFMO3 has not been solved due to difficulties in the crystallization of microsomal, membrane-bound proteins [10]. In the past, several reports have demonstrated a successful increase in the solubility of membrane proteins by deleting the anchor that binds them to the membranes [11-13]. In 1991 Ozols [14] revealed that the C-terminus of FMO2 is very hydrophobic and it could anchor the protein to the membrane. More recently, Krueger and co-workers [15] reported on the expression and purification attempts of a soluble rabbit FMO2 by deleting 26 amino acids from the C-terminus region presumed to function as the membrane anchor.

In the present study, based on the hydrophobic nature of the C-terminus of the protein, a truncated hFMO3 was engineered by deleting the C-terminal region at different amino acid positions. The protein sequence with a 17 amino acid deletion (tr-hFMO3) was expressed and purified. The tr-hFMO3 proves to be detached from the membrane and it is not only fully active towards well-known marker substrates such as benzydamine and sulindac sulfide, but also newly discovered Aurora kinase inhibitors such as Tozasertib [16] and Danusertib [17].

The use of this soluble form of the hFMO3 enzyme as opposed to the usual microsomal preparations can be advantageous for *in vitro* drug metabolism studies that are a requirement in the early phases of drug development by pharmaceutical industry. These studies are important not only in revealing potential metabolites but also allowing for elucidation of their toxicity and any possible adverse drug reactions.

2. Experimental Procedures

2.1. Reagents

Methimazole (MMI), sulindac, sulindac sulfide, benzydamine, benzydamine N-oxide, FAD, Igepal, acetonitrile, methanol, NADPH and 5,5'-dithiobis(2-nitrobenzoate) and salts were purchased from Sigma-Aldrich (Italy). Tozasertib and Danusertib were purchased from Aurogene (Italy).

2.2. Molecular Dynamics

Molecular dynamics in membrane was done using the YASARA [18] “md run membrane” for 4 nanoseconds. YASARA automatically identified the C-terminus of the hFMO3 as a hydrophobic exposed region bound to the membrane and constructed a membrane environment accordingly. YASARA unequivocally assigned the sequence between residues ARG 504 and THR 532 to a putative transmembrane helix and the protein was automatically rotated in order to fill the simulation cell volume with physiological solution and lipid content accordingly to the C-terminal helix. For all simulations, AMBER 03 forcefield was applied.

2.3. Protein-ligand interaction study

AutoDock 4.0 [19], embedded into the YASARA Structure package, was used to dock benzydamine, sulindac sulfide, tozasertib and danusertib to the refined model. Danusertib and tozasertib were obtained from the HIC-UP [20] database for hetero-compounds and were utilized with the same coordinates as they can be found in the co-crystals with the kinase domain of Abl

[21] and Aurora kinase AurA [22], respectively. Benzydamine and sulindac sulfide were obtained from PubChem (www.ncbi.nlm.nih.gov/pccompound) and were geometrically optimized using MOPAC [23] also embedded in the YASARA package. The optimized ligand molecules were docked into the refined protein model by running twenty-five of Global Docking centering a 15x15x15 Å simulation cell on the FAD group. In YASARA, docking runs of the ligand to receptor yield results sorted by binding energy where more positive energies indicate stronger binding and negative energies equate to no binding. After global docking the best binding mode (pose) was selected based on the best binding energy. The complexes were then subjected to 999 runs of Local Docking yielding the final docked binding modes.

The global docking experiment, in which the drug is originally outside the simulation box and is placed inside the cell by exploiting the autodock algorithm, resulted in a series of binding modes classified by the binding energy outputs. Among these binding modes the complex protein-ligand bearing the highest binding energy calculated by YASARA [18] as the mechanical energy required for disassembling a whole into separate parts, was selected and refined by local docking. In local docking experiments the ligand is within the simulation cell and the possible conformations are assayed for a maximum of 999 runs and the results are again sorted by binding energy. In this case, since the starting positions of the ligand inside the simulation box are often random and it is probable that a certain pose/binding mode could never be detected, molecular dynamics simulations were applied to better accommodate the ligand inside the pocket.

2.4. Cloning, expression and purification

WT hFMO3 was cloned in the expression vector pJL2 [24] using the two restriction enzymes XbaI and HindIII previously [25]. The plasmid was digested by these two enzymes and the gene was amplified with the primers: 5' AGT TCC CAG AAC TCT AGA ATG GGG AAG AAA GTG GCC ATC 3' as forward for all the reactions, 5' GCT CAT CGA AGC TTT TAA TGG TGA TGG TGC CGG TCC CAC TGG GTC AGT AT 3' as a reverse for 493X, 5' GCT CAT CGA AGC TTT TAA TGG TGA TGG TGT CTC CCG ACC ACT CGT GTC TG 3' as a reverse

for 505X and 5' GCT CAT ATA AGC TTT TAA TGG TGA TGG TGC AGC CAA TGG AAA AAG AAG CAA GGC 3' as a reverse for 516X (tr-hFMO3). All the reverse primers contained the sequence coding for a 4His-tag (5' ATGGTGATGGTG 3'), to assist in the purification. The amplified genes were then digested with the restriction enzymes XbaI and HindIII and cloned back into pJL2.

Wild type and the tr-hFMO3 were expressed in *E. coli* JM109 cells and grown 24 hr post-induction. WT protein was purified from the membrane fractions whereas the truncated hFMO3 was purified from the cytosolic fraction. All other purification steps were identical. Both proteins were purified via Ni affinity chromatography. Spectra of the eluted fractions (with 40mM histidine) were recorded using a diode array HP-8453E spectrophotometer. FAD containing fractions with the characteristic absorption peaks at 375 and 442 nm were pooled and exchanged to storage buffer (100 mM potassium phosphate buffer pH 7.4, 20% glycerol and 1 mM EDTA) by 30 kDa cutoff Amicon membranes and stored at -20°C.

2.5. FAD content determination

The concentration of holo hFMO3 was determined by spectroscopy with the peak absorbance at 450 nm and an extinction coefficient of $11900 \text{ M}^{-1} \text{ cm}^{-1}$, as previously described for other flavin-containing enzymes [26]. This value was also used for the determination of the enzyme concentration under non-denaturing conditions. In addition to the active enzyme (flavin-bound) concentration, the total hFMO3 protein concentration for the final purified protein was determined using both absorbance at 280 nm (extinction coefficients of $87520 \text{ M}^{-1} \text{ cm}^{-1}$ and $87485 \text{ M}^{-1} \text{ cm}^{-1}$ for WT and tr-hFMO3, respectively) and Bradford assay.

2.6. Far-UV circular dichroism analysis

Far UV circular dichroism experiments were performed on the WT and tr-hFMO3 at room temperature (Jasco-J600 spectropolarimeter). In order to improve the signal-to-noise ratio, several (3-4) spectra were accumulated and averaged for each sample. The measurements were carried out using 5 μM of protein and quartz cuvettes with a path length of 0.1 cm for the far UV

(200–250 nm). Secondary structure prediction for both enzymes was performed using the K2D2 algorithm [27].

2.7. FAD aerobic reduction

The protein was diluted to 7 μM in 50 mM potassium phosphate buffer pH 7.4 at 10°C. After the addition of aerated NADPH spectra were recorded using a Hewlett-Packard diode array spectrophotometer. The re-oxidation of the enzyme was followed by measuring the increase in absorbance at 442 nm.

2.8. Enzyme-substrate incubations and HPLC analysis

WT and tr-hFMO3 catalyzed S-oxygenation of MMI was monitored using the method previously described [28,29] at 37°C. Rates of N-oxygenation of benzydamine [30] and S-oxygenation of sulindac sulfide [31] for WT and tr-hFMO3 were determined using HPLC methods described previously. A typical incubation mixture consisted of 50 mM potassium phosphate buffer (pH 7.4), NADPH, the substrate and 0.17 μM of purified enzyme in a final volume of 0.20 ml. Incubations were carried out at 37°C for 10 min: the linearity of product formation was confirmed with purified hFMO3 preparations for 20 min. The reaction was terminated by the addition of 0.10 ml of ice-cold acetonitrile for benzydamine and by adding 50 μL of 50% phosphoric acid and 1.0 ml of ethyl acetate for sulindac sulfide. For sulindac sulfide, after centrifugation at 2000g for 10 min, the organic phase was transferred to a clean tube and evaporated in a vacuum pump. The residue was dissolved in 0.20 ml of mobile phase (50% acetonitrile in 25 mM potassium phosphate buffer, pH 3.0) and introduced into the HPLC apparatus (Agilent-1200 series). For benzydamine the aqueous supernatant was centrifuged at 2000g for 10 min and was subjected to HPLC equipped with a 4.6 x 150 mm 5 μm Eclipse XDB-C18 column at room temperature and the UV-visible detector was set at 308 nm. A sample of 20 μl was injected and the separation was performed using a mobile phase of 32% acetonitrile and 68% 50 mM KH_2PO_4 pH 7.4 at a flow rate of 1.4 ml/min, which was increased to 1.8 ml/min after 7 minutes. The formation of sulindac sulfoxide was monitored at 360 nm [31]. The kinetic

analysis of N or S-oxygenation was carried out using a nonlinear regression analysis program (SigmaPlot).

In the case of hFMO3-catalyzed N-oxygenation of tozasertib and danusertib, a typical incubation mixture consisted of 50 mM potassium phosphate buffer (pH 7.4), NADPH, the substrate and 0.17 μ M of purified enzyme in a final volume of 0.20 ml. Incubations were carried out at 37°C for 10 min: the linearity of product formation was confirmed with purified hFMO3 preparations for 20 min. The incubation was terminated by the addition of 0.10 ml of ice-cold methanol. The aqueous supernatant was centrifuged at 2000g for 10 min and was subjected to HPLC equipped with an analytical C18 column (4.6 x 150 mm, 5 μ m). A 75 μ l sample was injected and the separation was performed using a mobile phase of 70% methanol and 30% water at a flow rate of 1.0 ml/min. The formation of tozasertib N-oxide was monitored at the wavelength of 250 nm while the danusertib N-Oxide product was monitored at 295 nm.

2.9. Enzyme interaction with the lipid bilayer (QCM-D)

Small Unilaminar Vesicles (SUV) were formed by tip sonicating EggPC (5 mg/ml, Avanti Lipids) in MOPS buffer (20 mM MOPS pH 7.4, 30 mM Na₂SO₄) for 30 minutes at 4 °C until clear. Tip particles were removed by spinning the sample for 5 min. at 14,500 g. SUVs were stored at 4 °C and used within two days. Directly before the experiment, the sample was diluted to 0.5 mg/ml in Milli-Q water (18.2 M Ω cm²).

SiO₂-coated crystals (Q-sense) were bath sonicated in 0.4% SDS (Sigma) for 30 min., followed by sonication in Milli-Q for another 30 min. The crystals were then further treated for 30 min with UV/ozone (UV/ozone cleaning system, low pressure quartz-mercury vapor lamp emitting 254 and 185 nm UV, UVOCS, Montgomeryville) and installed in the Quartz-Crystal Microbalance with Dissipation (QCM-D) equipment (Q-Sense E4, Q-Sense AB, Gothenburg, Sweden). After equilibrating the crystals with buffer (all experiments were performed with a flow rate of 70 μ L/min), they were incubated with the EggPC SUV (0.5 mg/ml) until a stable response was observed (typically 10 min), indicating that a planar solid-supported bilayer is formed. The

QCM-D crystals were then rinsed with Milli-Q water, followed by MOPS buffer. Finally, the crystals were incubated with 1 μ M hFMO3 and tr-hFMO3 in MOPS buffer. Human FMO3 was made up from a 100 μ M stock solution containing 0.1% (v/v) of the detergent, Igepal, thus reducing the Igepal to about 0.001% (v/v). Control experiments were performed to check that these levels of detergent in the hFMO3 sample do not disrupt the sBLM and no effect was observed for Igepal up to 0.005% (v/v).

3. RESULTS

3.1. Membrane anchoring and construction of the truncated hFMO3

In order to facilitate the *in vitro* experimental determination of drug metabolism by hFMO3 we identified and eliminated its membrane anchor producing a soluble and active enzyme. It has previously been hypothesized that the C-terminal region of hFMO3 is responsible for its anchoring to the membrane [9,14], therefore we analysed the primary sequence of this enzyme and the resulting hydropathy plot (Figure 1) pointed to a putative transmembrane region starting from residue 516 in the C-terminus of this protein. In addition to the hydropathy plot, *in silico* molecular dynamics experiments were also carried out (data not shown) which also demonstrated the presence of a putative transmembrane helix consisting of amino acid residues between 504 and 532 in the C-terminus.

Based on the above-mentioned analyses a series of C-terminus truncated hFMO3 sequences were generated and cloned in the expression vector pJL2. The purpose of the truncation was to interrupt the hFMO3 gene at the level of the C-terminal region of the protein and to obtain a more soluble enzyme with less affinity to the hydrophobic membrane. A stop codon was therefore inserted in the hFMO3 gene at positions codifying for: ARG 492, LYS 505 and LYS 516. Although all the latter constructs were produced, only the one with the least number of amino

acid deletions (i.e. stop codon at LYS 516) was expressed and purified. This truncated enzyme (tr-hFMO3) was used for all the subsequent *in vitro* characterisation experiments.

3.2. Purification and spectroscopical characterisation of the truncated hFMO3

Wild type hFMO3 was heterologously expressed in *E. coli* and purified to serve as a control for the truncation experiments. Purification started by loading the membrane fraction onto a DEAE ion exchange chromatography that cleared the bacterial crude extract, not retaining hFMO3 at pH 7.4 followed by a Ni affinity column. The same protocol was applied to the tr-hFMO3, but in this case the protein was found in the cytosolic fraction. The yield of pure protein was determined using the absorbance of the aromatic residues at 280 nm in combination with the Bradford protein assay, leading to approximately 12-13 mg per litre of culture in case of the WT protein and 9-10 mg per litre of culture for the truncated form. SDS-PAGE analysis of the Ni-affinity purified samples showed a band at approximately 60 kDa (Fig. 2A) in good agreement with the molecular weight calculated from the amino acid sequence of hFMO3.

Both purified WT and tr-hFMO3 exhibited a yellow colour typical of FAD. The elution profile showed a clear correlation between the total protein content and the FAD absorbance at 450 nm. The FAD content of the purified proteins (holoprotein-determined by absorbance at 450 nm) was compared to the total hFMO3 concentration (holo and apoprotein-determined at 280 nm). The molar ratios showed 85% and 91% of holo-protein content for WT and tr-hFMO3, respectively.

The purified proteins were further characterised by spectroscopy. In the first instance, reduction of the WT and tr-hFMO3 were carried out aerobically in the presence of NADPH (in the absence of the substrate) that rapidly bleaches the protein solutions. Figure 2C and 2D show the oxidised spectra for wild type and tr-hFMO3 with the maxima at 372 and 442 nm together with the reduced forms. As can be seen in the figure, the truncation has had no effect on the NADPH binding and subsequent reduction of the protein.

In order to confirm that the truncation of the C-terminus of hFMO3 did not affect the overall folding of the protein, the far-UV CD spectra of tr-hFMO3 were recorded and compared to those

of the wild type protein. Figure 2B shows the overlapped far UV CD spectra of WT and tr-hFMO3. As can be seen in the latter figure, the structure of tr-hFMO3 has a reduced helical content as verified by the lower CD intensity of the two peaks at 208 and 222 nm. However, the deletion of the last 17 amino acids of the protein sequence has not compromised the overall secondary structure of the enzyme. Analysis of the far-UV CD spectra by the K2D2 software [27] led to the results shown in Table 1 where both proteins showed a predominantly α -helical secondary structure and as expected a 4% reduction in the alpha helices present in tr-hFMO3.

The fact that tr-hFMO3 was found in the cytosolic rather than in the membrane fraction suggests that this truncated protein has lost the ability to interact with the lipid bilayer. Solid-supported bilayer lipid membranes (sBLM) are very useful in studying the interaction of a protein with model membranes, as protein adsorption and interaction can be followed with Quartz-Crystal Microbalance with Dissipation (QCM-D) measurements. After the formation of a sBLM, the typical QCM-D signal was observed due to the mass of the lipid membrane which changes the QCM-D frequency with -24 Hz and without changing the energy dissipation [32]. Upon addition of 1 μ M tr-hFMO3, a sub-monolayer ($< 1/3$ of a full monolayer) adsorbs on the lipid bilayer, which detaches again after rinsing the crystal with buffer (Figure 3, phase 3, bottom graph). This confirms that tr-hFMO3 has retained little or no affinity for lipid bilayer.

On the other hand, addition of the full-length WT hFMO3 resulted in a rapid decrease in frequency, indicating an increase in mass and thus a strong interaction between the sBLM and WT hFMO3 (Figure 3, phase 2, top graph). However, this was immediately followed by a loss of material from the surface. We ascribe this behaviour to the ability of hFMO3 to strip the sBLM off the surface. This hypothesis was confirmed by fluorescent microscopy using fluorescently labelled lipids, which showed that addition of hFMO3 resulted in the destruction of the sBLM and formation of lipid vesicles and aggregates loosely associated with the SiO₂ surface. Interestingly, when the surface was rinsed with buffer (Figure 3, phase 3), the loosely bound lipid

material reabsorbed on the surface and the large increase in mass suggested that a significant amount of hFMO3 co-immobilised on the surface. Fluorescent microscopy confirmed that a partial fluid sBLM is formed after rinsing the surface with buffer (data not shown).

QCM-D provides information regarding the adsorption kinetics and relative mass uptake, and additionally, the dissipation reveals intermediate stages of vesicle adsorption [33]. Figure 5B shows how QCM-D responses of sBLMs are different after the addition of the WT or tr-hFMO3 enzymes. Both frequency and dissipation signals display a different attitude: WT determines a net change after absorption indicating a strong interaction between the enzyme and the membrane while tr-hFMO3 does not change either frequency or dissipation.

3.3. Metabolism of drugs by the truncated hFMO3

Further characterization of the tr-hFMO3 included measuring its monooxygenation activity and comparing it to the WT enzyme. For this reason the oxidation of methimazole, benzydamine and sulindac sulfide were investigated. K_m and V_{max} data obtained for tr-hFMO3 are reported in Table 2 where the values are compared with those measured for WT hFMO3. Apparent K_m values for WT and tr-hFMO3 for benzydamine N-oxygenation were $56 \pm 8 \mu\text{M}$ and $45 \pm 8 \mu\text{M}$ respectively, while apparent V_{max} values of 9 for WT and 11 for tr-hFMO3 were obtained. Similar results were obtained using sulindac sulfide S-oxygenation as a marker reaction catalyzed by WT and tr-hFMO3 with K_m values of $25 \pm 7 \mu\text{M}$ and $25 \pm 4 \mu\text{M}$, respectively. The K_m values obtained for both these known substrates are similar to previously published data using microsomal hFMO3 preparations [34-36].

In all cases the kinetic values measured show that the tr-hFMO3 is not only fully active but also has the same activity range as those measured for the WT protein.

The kinetic characterization of the tr-hFMO3 was taken one step further by looking at the identity of the products formed by the turnover of the known substrates (drugs) of this enzyme. After each set of reactions at 37 °C in the presence of NADPH, the product(s) was separated by HPLC and the data obtained are shown in Figure 4A-F. As can be seen from the latter figure, the

expected benzydamine N-oxide and suldinac were detected with retention times of 4.0 min and 5.2 min, respectively.

The activity of the tr-hFMO3 enzyme was also tested on tozasertib and danusertib that are involved in cancer treatment as Aurora kinase inhibitors and for which no data on recombinant hFMO3 turnover is available to date. Again in this case the product(s) were separated using HPLC and the data are shown in Figure 4G-N. The results show that both WT and tr-hFMO3 are able to metabolize these two drugs since extra peaks are observed in the HPLC chromatograms with shorter retention times of 4.1 min for “tozasertib N-oxide” and 3.7 min for “danusertib N-oxide” [37,38].

However, chemical standards for N-oxides of tozasertib and danusertib are not commercially available and in order to ascertain the identity of the products seen in Figure 4 (H-I-M-N) further characterization was carried out using LC-MS. The fragmentation of the reaction products of tozasertib and danusertib corresponded to those obtained by Ballard and co-workers [37] and Cohen’s group [38] respectively, confirming that the products were N-oxides of the two kinase inhibitors.

Overall, the data presented demonstrate that the reactions carried out by the tr-hFMO3 are the same as those performed by the WT enzyme.

3.4. Molecular docking

For enzymes where currently the three-dimensional crystal structure is unavailable, molecular modelling studies can enable the development of models that allow predictions of new substrates and design of modulators of enzyme function. To this end, a molecular model of hFMO3 was constructed using the crystal structures of FMO proteins from *Methylophaga* sp. Strain SK1 (PDB: 2VQ7) [39] and *Schizosaccharomyces pombe* (PDB: 2GV8) [40] together with a Baeyer-villiger monooxygenase from *Thermobifida fusca* (PDB:1W4X) [41].

As previously hypothesized [9], hFMO3 is thought to act as a loaded gun where the FAD is

reduced by NADPH and it is ready to oxygenate any N, S or P containing soft nucleophiles. This mechanism is crucial for the understanding of the active site architecture of the enzyme and the key role exerted by NADPH in catalysis and stabilization. For this reason all docking experiments were carried out in the presence of NADP⁺ by placing the simulation cell around the isoalloxazinic ring of FAD including all the residues located on the broad substrate exposed cavity of hFMO3 predicted by molecular modelling.

In order to confirm the feasibility of using our 3D generated model for predictions of new substrates of hFMO3, initially docking experiments were performed with the two well-characterized substrates benzydamine and sulindac sulfide, the former N-oxidized and the latter S-oxidized by hFMO3, for which *in vitro* catalysis data were already reported in the previous section.

Docking of benzydamine (an anti-inflammatory drug) and Sulindac sulfide (a non-steroidal anti-inflammatory drug) resulted in complexes with binding energies of 8.46 kcal/mol and 8.90 kcal/mol, respectively. As can be seen from Figure 5A-B residues LYS 64, ASN 194 and LEU 375 are responsible for the stabilization of both these substrates inside the hFMO3 active site. All these residues interact with the ligands by giving CH/ π interactions. As expected the known N-oxidation site of benzydamine is located at the aliphatic chain of this tertiary amine at a distance of 3.5 Å from the C4 of the FAD isoalloxazine ring (Fig. 5A). As for the S-oxidation site of the sulindac sulfide, a similar distance of 3.4 Å from the C4 of the isoalloxazine ring was measured (Fig. 4B).

Both known substrates of hFMO3, benzydamine and sulindac sulfide, interact correctly with its active site by not only resulting in a complex that is energetically favoured, but also by interacting with the enzyme in the expected binding mode for catalysis. These results give strength to our 3D generated model and therefore in a subsequent round of docking simulations the two Aurora kinase inhibitors involved in cancer treatment namely tozasertib and danusertib were tested.

Docking results showed stronger binding energies for both kinase inhibitors compared to those calculated for the known substrates: 9.83 kcal/mol and 11.02 kcal/mol for tozasertib and danusertib, respectively. Figure 5C-D show how residues LYS 64, GLU 65, MET 67/MET 66 and ASN 194 are responsible for the stabilization of these kinase inhibitors inside the active site of hFMO3. All these residues interact with both substrates by giving CH/ π interactions and the putative N-oxidation sites are at a distance of 3.1 Å for tozasertib and 2.7 Å for danusertib from the C4 of the isoalloxazine ring. In the case of danusertib an extra residue, TYR 462, is involved in the binding mode shown in Figure 4D. The latter residue interacts with the ligand through π / π interactions leading to the highest calculated binding energy amongst the four drugs tested.

In all the docking experiments reported above, distances of <4 Å between N or S oxidation sites of the substrates and the C4 of the FAD isoalloxazine ring were measured. As mentioned earlier, in these experiments the oxidised structure of FAD was used due to the fact the reduced C4a-hydroperoxyflavin intermediate of FMO enzymes has never been characterised by crystallography and therefore not present in the Protein Data Bank. However, such an intermediate has been observed by single-crystal spectroscopic methods and 1.86 Å resolution X-ray crystal structure in the bacterial Choline oxidase, a flavoprotein [42]. Density functional theory calculations carried out for the intermediate seen in Choline oxidase led to measured distance of 3.7 Å (between the oxygen atom of the C4a-OO(H) and the ligand) that is very similar to the distances measured in the docking experiments reported here.

All in all the docking experiments yielded a series of binding modes for each of the docked substrates that were consistent with the correct binding mode of these molecules in the active site of hFMO3 compatible with the nature of the product formed: the nitrogen or the sulphur atom that is the site of the catalysis is not only facing the FAD isoalloxazine ring but it is also within acceptable distance (<4 Å) from the FAD reactive site involved in monooxygenation. These results give strength to the 3D generated model that can be further used for screening of other “probable” substrates of this enzyme.

CONCLUDING REMARKS

To improve the efficiency of drug development by pharmaceutical companies many of them carry out *in vitro* drug metabolism studies using purified enzymes. In the case of hFMO enzymes these studies are currently performed with microsomal suspensions. In this work we have shown that it is possible to engineer and purify a truncated version of hFMO3 enzyme that has the same catalytic properties of that of the wild type enzyme with added advantage of being also more soluble.

The hydropathy plot of the amino acid sequence of hFMO3 identified the C-terminus as a membrane bound helix. On this basis, a truncated form of hFMO3 was engineered and purified from the cytosolic fraction. Spectroscopic characterization and secondary structural measurements together with kinetic assays indicate that tr-hFMO3 is very similar to the full-length WT enzyme. Moreover, molecular dynamics in the membrane and QCM-D experiments showed that tr-hFMO3 has a decreased affinity for lipid membranes. These data confirm the role of the C-terminus of hFMO3 in membrane binding and suggest that deletion of the helix does not affect folding, stability and catalytic properties of the enzyme.

A 3D model of hFMO3 was also generated and docking experiments with both known and probable substrates of this enzyme, namely, benzyamine, sulindac sulfide, tozasertib and danusertib were carried out. *In vitro* catalysis experiments of the wild type protein with tozasertib and danusertib confirmed the docking results giving further strength to the model that can be used in the future for screening of other candidate substrates of this enzyme.

Acknowledgements

The authors thank Prof. Maffei (University of Torino) and Mr. Occhipinti for assistance with the mass spectrometry experiments.

REFERENCES

- [1] Cashman, J.R. and Zhang J. Human flavin-containing monooxygenase. *Annu. Rev. Pharmacol. Toxicol* 2006; 46: 65-100.
- [2] Krueger SK, Williams DE. Mammalian flavin-containing monooxygenase: structure/function, genetic polymorphism and role in drug metabolism. *Pharmacol Ther* 2005;106:357-87.
- [3] Cashman, J.R. *Curr. Human flavin-containing monooxygenase: Substrate specificity and role in drug metabolism. Drug Metab.* 2000;1:181-91.
- [4] Kang, J.H., Chung, W.G., Lee, K.H., Park, C.S., Kang, J.S., Shin, I.C. et al. Phenotypes of flavin-containing monooxygenase activity determined by ranitidine N-oxidation are positively correlated with genotypes of linked FMO3 gene mutations in a Korean population. *Pharmacogenetics* 2000;10: 67–78.
- [5] Koukouritaki, S.B. and Hines. Flavin-containing monooxygenase genetic polymorphism: impact on chemical metabolism and drug development R.N. *Pharmacogenomics* 2005; 6:807-22.
- [6] Reddy, R.R., Ralph, E.C., Motika, M.S., Zhang, J. and Cashman, J.R. *Drug Metab. Dispos.* 2010;38: 2239-45.
- [7] Ziegler, D.M. Recent studies on the structure and function of multi-substrate flavin-containing monooxygenases. *Annu. Rev. Pharmacol. Toxicol.* 1993; 33:179-99.
- [8] Cashman, J.R. Structural and catalytic properties of the mammalian flavin-containing monooxygenase. *Chem. Res. Toxicol.* 1995;8; 165-81.
- [9] Ziegler DM. An overview of the mechanism, substrate specificities, and structure of FMOs. *Drug Metab Rev* 2002;34:503–511.
- [10] Lee, J.K. and Stroud, R.M. Unlocking the eukaryotic membrane protein structural proteome. *Curr. Opin. Struct. Biol.* 2010; 20:464-70.
- [11] Schoch, G.A., Yano, J.K., Wester, M.R., Griffin, K.J., Stout, C.D. and Johnson, E.F. Structure of human microsomal cytochrome P4502C8 - Evidence for a peripheral fatty acid binding site *J. Biol. Chem.* 2004; 279: 9497-9503.
- [12] Ekroos, M. and Sjogren, T. Structural basis for ligand promiscuity in cytochrome P450 3A4. *Proc. Natl. Acad. Sci. USA* 2006;103:13682.
- [13] Sansen, S., Yano, J.K., Reynald, R.L., Schoch, G.A., Griffin, K.J., Stout, C.D. and Johnson, E.F. Adaptations for the oxidation of polycyclic aromatic hydrocarbons exhibited by the structure of human P450 1A2. *J. Biol. Chem.* 2007;282:14348-14355.
- [14] Ozols, J. Multiple forms of liver microsomal FMO- Complete covalent structure of form-2.

Arch. Biochem. Biophys. 1991;290:103-15.

- [15] Krueger, S.K., Vandyke, J.E., Williams, D.E. and Hines, R.N. C-terminal truncation of rabbit flavin-containing monooxygenase isoform 2 enhances solubility. Arch Biochem Biophys. 2006; 450:149-56.
- [16] Harrington, E.A., Bebbington, D., Moore, J., Rasmussen, R.K., Ajose-Adeogun, A.O., Nakayama, T., et al. VX-680, a potent and selective small-molecule inhibitor of the Aurora kinases, suppresses tumor growth in vivo. Nature Med. 2004;10:262-7.
- [17] Carpinelli, P., Ceruti, R., Giorgini, M.L., Cappella, P., Gianellini, L., Croci, V., et al. PHA-739358, a potent inhibitor of Aurora kinases with a selective target inhibition profile relevant to cancer. Mol. Cancer Therap. 2007;6: 3158-68.
- [18] Krieger, E. and Vriend, G. Model@Home: distributed computing in bioinformatics using a screensaver based approach. Bioinformatics 2002;18:315-318.
- [19] Goodsell, D.S., Morris, G.M. and Olson, A.J. Automated docking of flexible ligands: Applications of AutoDock. J. Mol. Recognit. 1996;9: 1-5.
- [20] Kleywegt, G.J. Separating model optimization and model validation in statistical cross-validation as applied to crystallography. Acta Cryst. 2007;63:94-100.
- [21] Modugno, M., Casale, E., Soncini, C., Rosettani, P., Colombo, R., Lupi, R., et al. Crystal structure of the T315I Abl mutant in complex with the aurora kinases inhibitor PHA-739358. Cancer Res. 2007;67:7987-90.
- [22] Zhao, B., Smallwood, A., Yang, J., Koretke, K., Nurse, K., Calamari, A., Kirkpatrick, R.B. and Lai, Z. Modulation of kinase-inhibitor interactions by auxiliary protein binding: Crystallography studies on Aurora A interactions with VX-680 and with TPX2. Protein Sci. 2008;17:1791-97.
- [23] Stewart, J.J. special issue - MOPAC - A Semiempirical molecular-orbital program. J. Comput. Aided Mol. Des. 1990;4:1-45.
- [24] Dong, J.S. and Porter T.D. Coexpression of mammalian cytochrome P450 and reductase in Escherichia coli. Arch. Biochem. Biophys. 1996;327:254-259.
- [25] Sadeghi, S.J., Meirinhos R., Catucci G., Dodhia V.R., Di Nardo G. and Gilardi G. Direct Electrochemistry of Drug Metabolizing Human Flavin-Containing Monooxygenase: Electrochemical Turnover of Benzydamine and Tamoxifen. J. Am. Chem. Soc. 2010;132:458-59.
- [26] Wagner, M.A., Khanna, P. and Jorns, M.S. Structure of the flavocoenzyme of two homologous amine oxidases: Monomeric sarcosine oxidase and N-methyltryptophan oxidase. Biochemistry 1999;38:5588-95.
- [27] Perez-Iratxeta, C. and Andrade-Navarro, M.A. K2D2: estimation of protein secondary

structure from circular dichroism spectra. *BMC. Struct. Biol* 2008;8:25-29.

- [28] Dixit, A. and Roche T.E. Spectrophotometric assay of the flavin-containing monooxygenase and changes in its activity in female mouse liver with nutritional and diurnal conditions. *Arch. Biochem. Biophys.* 1984;233:50-63.
- [29] Motika, M.S., Zhang, J., Zheng, X., Riedler, K. and Cashman, J.R. Novel variants of the human flavin-containing monooxygenase 3 (FMO3) gene associated with trimethylaminuria. *Mol. Genet. Metab.* 2009;97: 128-135.
- [30] Yeung C.K., Adman, E.T. and Rettie, A.E. Functional characterization of genetic variants of human FMO3 associated with trimethylaminuria. *Arch. Biochem. Biophys.* 2007;464:251-59.
- [31] Hamman, M.A, Haehner-Daniels, B.D., Wrighton, S.A., Rettie A.E. and Hall S.D. Stereoselective sulfoxidation of sulindac sulfide by flavin-containing monooxygenases - Comparison of human liver and kidney microsomes and mammalian enzymes. *Biochem. Pharmacol.* 2000;60:7-17.
- [32] Richter, R.P., Bérat, R. and Brisson, A.R. Formation of solid-supported lipid bilayers: An integrated view. *Langmuir* 2006; 22:3497-3505.
- [33] Dodd, C.E., Johnson, B.R., Jeuken, L.J.; Bugg, T.D., Bushby, R.J. and Evans, S.D. Native *E. coli* inner membrane incorporation in solid-supported lipid bilayer membranes. *Biointerphases* 2008; 3: FA59-67.
- [34] Lang, D. H. and Rettie, A. E. J. In vitro evaluation of potential in vivo probes for human flavin-containing monooxygenase (FMO): metabolism of benzydamine and caffeine by FMO and P450 isoforms. *British J. Clin. Pharmacol.* 2000; 50: 311-14.
- [35] Stormer, E., Roots, I. and Brockmoller, J. Benzydamine N-oxidation as an index reaction reflecting FMO activity in human liver microsomes and impact of FMO3 polymorphisms on enzyme activity. *British J. Clin. Pharmacol.* 2000; 50(6): 553-61.
- [36] Shimizu, M., Yano, H., Nagashima, S., Murayama, N., Zhang, J., Cashman, J.R. and Yamazaki, H. Effect of genetic variants of the human flavin-containing monooxygenase 3 on N- and S-oxygenation activities. *Drug Metab. Dispos.* 2007; 35(3): 328-30.
- [37] Ballard, J.E., Prueksaritanont, T. and Tang, C. Hepatic metabolism of MK-0457, a potent Aurora kinase inhibitor: interspecies comparison and role of human cytochrome P450 and flavin-containing monooxygenase. *Drug Metab. Dispos.* 2007; 35:1447-51.
- [38] Cohen, R.B., Jones, S.F., Aggarwal, C., von Mehren, M., Cheng, J., Spigel, D.R. et al. A phase I dose-escalation study of Danusertib (PHA-739358) administered as a 24-hr infusion with and without granulocyte colony-stimulating factor in a 14-day cycle in patients with advanced solid tumors. *Clin. Cancer Res.* 2009;15(21): 6694-6701.

- [39] Alfieri A., Malito E., Orru R., Fraaije M.W. and Mattevi A. Revealing the moonlighting role of NADP in the structure of a flavin-containing monooxygenase. *Proc. Natl. Acad. Sci. USA* 2008;105: 6572-7.
- [40] Eswaramoorthy, S., Bonanno, J.B., Burley, S.K. and Swaminathan, S. Mechanism of action of a flavin-containing monooxygenase. *Proc. Natl. Acad. Sci. USA* 2006;103:9832-37.
- [41] Malito, E., Alfieri, A., Fraaije, M.W. and Mattevi, A. *Proc. Natl. Acad. Sci. USA* 2004;101:13157-162.
- [42] Orville, A.M., Lountos, G.T., Finnegan, S., Gadda, G. and Prabhakar R. Crystallographic, spectroscopic, and Computational Analysis of a Flavin C4a-Oxygen Adduct in Choline Oxidase *Biochemistry* 2009;48:720-28.

TABLES

TABLE 1

Secondary structure content calculated from the far-uv CD spectra analysed by K2D2 software

Protein	Alpha helices	Beta strands	Random coils	Square distance	Max error
hFMO3	41%	17%	42%	32.2	0.08
tr-hFMO3	37%	20%	43%	29.8	0.08

TABLE 2

Kinetic parameters of hFMO3 and tr-hFMO3

	Methimazole			Benzylamine			Sulindac Sulfide		
	K_m	V_{max}	V_{max}/K_m	K_m	V_{max}	V_{max}/K_m	K_m	V_{max}	V_{max}/K_m
	μM	min^{-1}		μM	min^{-1}		μM	min^{-1}	
hFMO3	33±4	71±9	2.2	56 ± 8	9 ± 2	0.2	25 ± 7	108± 18	4.3
tr-hFMO3	35±6	69±12	2.0	45 ± 8	15 ± 7	0.3	22 ± 4	99 ± 21	4.5

FIGURE LEGENDS

FIGURE 1. Hydropathy Plot: the hFMO3 primary sequence was used to predict local hydrophobic patches using the DAS-TM plot: a clear hydrophobic sequence is shown at the C-terminus.

FIGURE 2. (A) 10% SDS-PAGE gel of purified hFMO3: Lane 1 shows the molecular weight markers, Lane 2 and 3 truncated and WT hFMO3, respectively. (B) Far-UV circular dichroism spectra of the WT hFMO3 (blue) and tr-hFMO3 (red). (C) Aerobic reduction of 5 μ M WT hFMO3 and (D) tr-hFMO3 in the presence of equimolar amounts of NADPH.

FIGURE 3. Quartz crystal microbalance-with dissipation (QCM-D) of the bilayer lipid membranes (sBLM) before (1) and after addition of hFMO3 (top) and tr-hFMO3 (bottom) (2) and subsequent rinsing (3). The data show the decreased ability of tr-hFMO3 to interact with the membrane.

FIGURE 4. HPLC chromatograms of incubations of benzydamine, sulindac sulfide, tozasertib and danusertib in the absence (A, D, G, L) and presence of tr-hFMO3 (B, E, H, M) and WT hFMO3 (C, F, I, N) enzymes.

FIGURE 5. Docked substrates into the active site of hFMO3 model. FAD is shown in yellow and the substrates are in dark blue. The S or N nucleophilic attack sites of the substrates are shown in magenta with the C4 of the FAD isoalloxazine ring in cyan. Residues interacting with the substrates are shown in red. Benzydamine (A), Sulindac (B), Tozasertib (C) and Danusertib (D).

Figure 1.

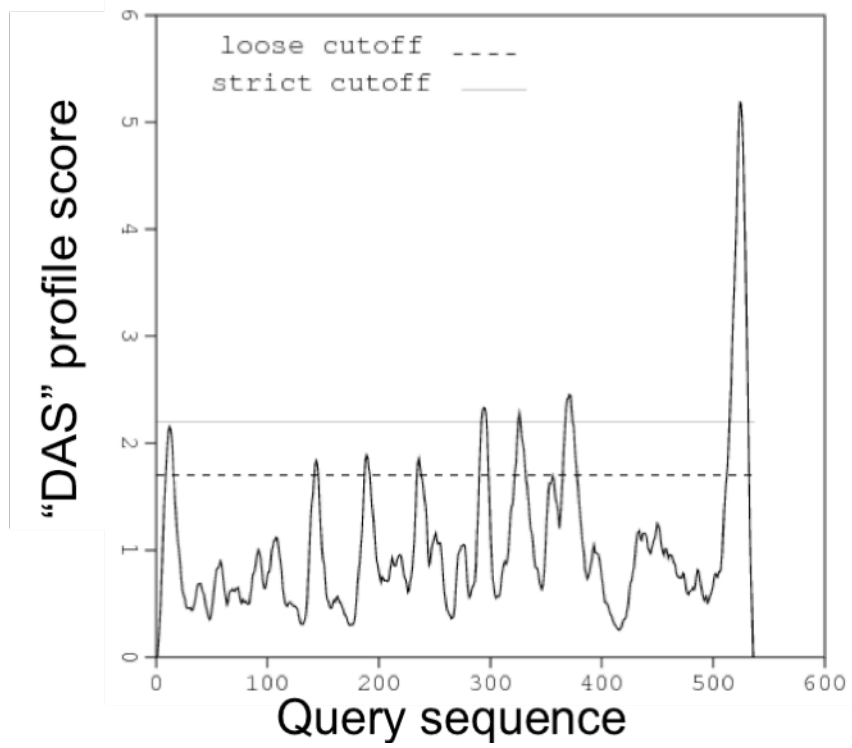


Figure 2.

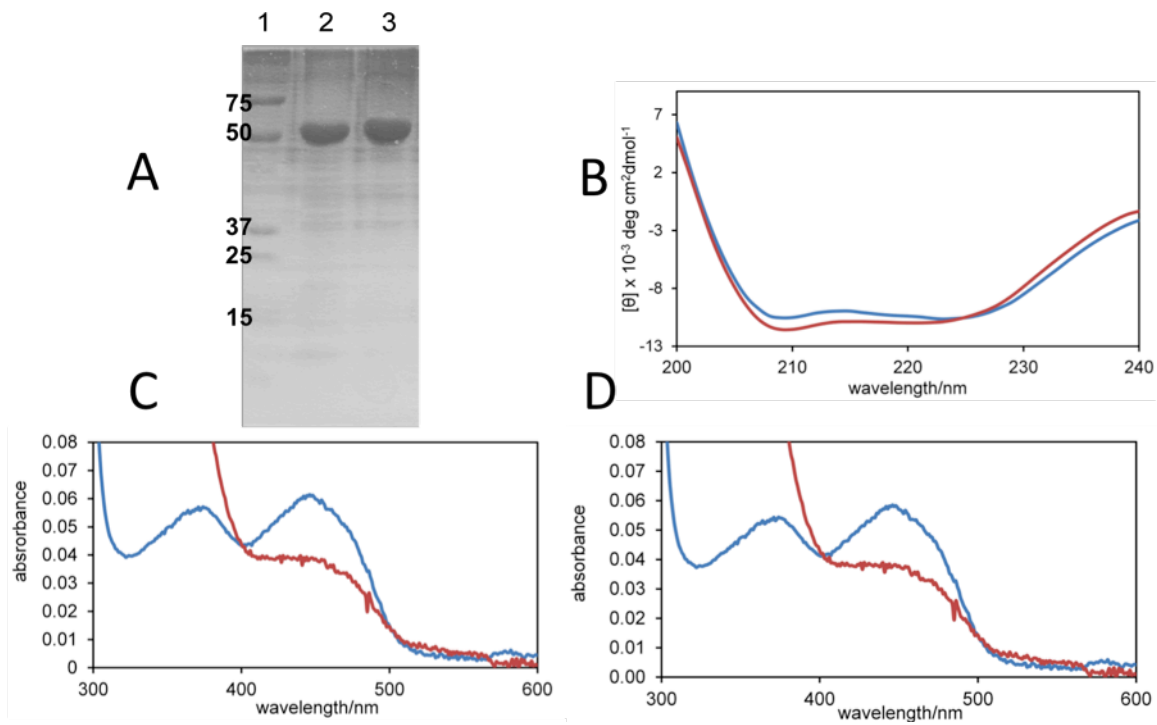


Figure 3.

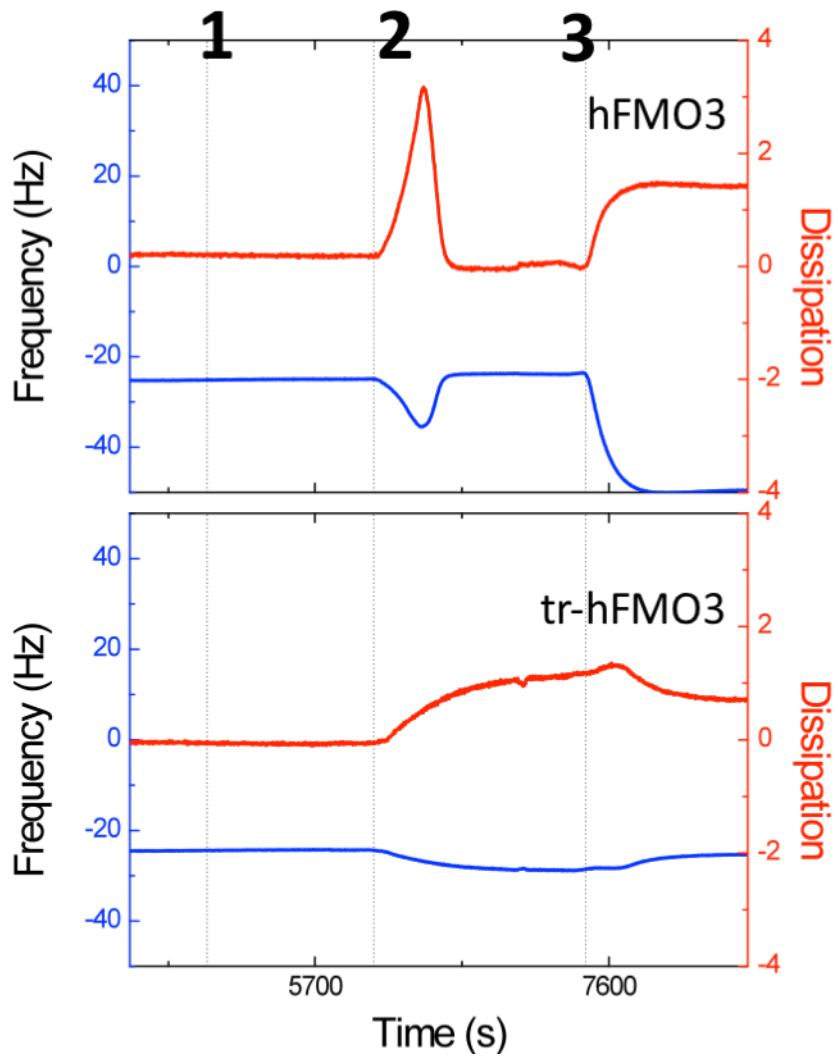


Figure 4.

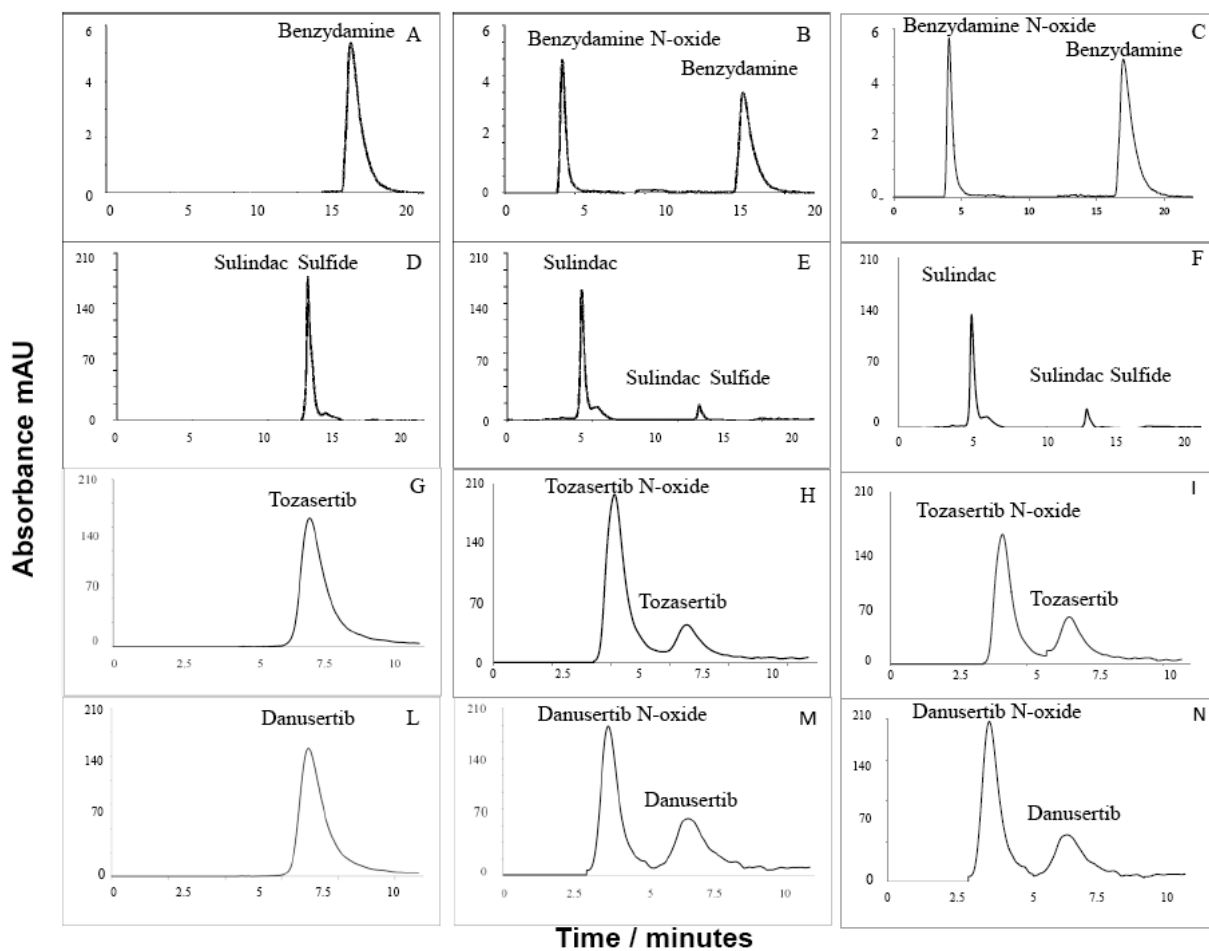


Figure 5.

